Special Issue

Comparing Optic Nerve Head Rim Width, Rim Area, and Peripapillary Retinal Nerve Fiber Layer Thickness to Axon Count in Experimental Glaucoma

Brad Fortune, Christy Hardin, Juan Reynaud, Grant Cull, Hongli Yang, Lin Wang, and Claude F. Burgoyne

Discoveries in Sight Research Laboratories, Devers Eye Institute and Legacy Research Institute, Legacy Health, Portland, Oregon, United States

Correspondence: Brad Fortune, Discoveries in Sight Research Laboratories, Devers Eye Institute and Legacy Research Institute, 1225 NE Second Avenue, Portland, OR 97232, USA; bfortune@deverseye.org.

Submitted: November 17, 2015
Accepted: April 11, 2016

Citation: Fortune B, Hardin C, Reynaud J, et al. Comparing optic nerve head rim width, rim area, and peripapillary retinal nerve fiber layer thickness to axon count in experimental glaucoma. *Invest Ophthalmol Vis Sci*. 2016;57:OCT404–OCT412. DOI:10.1167/iovs.15-18667

Purpose. We compare spectral-domain optical coherence tomography (SDOCT) measurements of minimum rim width (MRW), minimum rim area (MRA), and peripapillary retinal nerve fiber layer thickness (RNFLT) to complete orbital optic nerve axon counts in nonhuman primates (NHP) with unilateral experimental glaucoma (EG).

Methods. Biweekly SDOCT measurements of MRW, MRA, and RNFLT were acquired under manometric IOP control (10 mm Hg) in 51 NHP during baseline (mean ± SD, 5.0 ± 1.6 sessions) and after laser photocoagulation was applied to the trabecular meshwork of one eye to induce chronic IOP elevation. At the study endpoint (predefined for each NHP), 100% axon counts were obtained from each optic nerve.

Results. For SDOCT parameters at baseline, the correlation between the two eyes of each animal was strongest for RNFLT ($R = 0.97$) and MRW ($R = 0.97$), but lower for MRA ($R = 0.85$). At the final time point, average values in EG eyes relative to control eyes were: −22% for RNFLT, −38% for MRW, −36% for MRA, and −36% for optic nerve axons. The correlation with axon counts was strongest for RNFLT ($R = 0.81$), compared to MRW ($R = 0.72$, $P = 0.001$) or MRA ($R = 0.70$, $P = 0.001$). Diagnostic sensitivity was 75% for RNFLT, 90% for MRW, and 88% for MRA; all had 100% specificity.

Conclusions. Peripapillary RNFLT was correlated more closely with total orbital optic nerve axon count than were the ONH parameters MRW or MRA. This is likely because glaucomatous deformation (beyond axon loss alone) has a greater influence on the ONH parameters MRW and MRA than on RNFLT.

Keywords: glaucoma, optical coherence tomography, retinal ganglion cell axons, optic nerve head, retinal nerve fiber layer

Imaging techniques, such as optical coherence tomography (OCT), serve as an important aid in the diagnosis and management of glaucoma principally because they enable reliable, quantitative assessment of optic nerve head (ONH) and retinal nerve fiber layer (RNFL) structural integrity.[1–4] In this regard, OCT and other imaging techniques may help the clinician to detect the characteristic deformation of ONH connective tissue structures as well as the progressive degeneration of retinal ganglion cells and their axons, the primary cause of vision loss in glaucoma.

Chauhan and Burgoyne[5] recently advocated an improved approach to clinical assessment of the ONH for glaucoma. Among other aspects of their proposal, they argue that ONH neural rim tissue should be quantified using an OCT-derived parameter named Bruch's membrane opening-minimum rim width (BMO-MRW) because it has a stronger anatomical and geometric foundation than other existing methods. The concept of applying minimum distance mapping to ONH assessment for glaucoma diagnosis was introduced first by Povazay et al.[6] and later shown by Chen et al.[7] to have strong potential as a diagnostic parameter. Its advantages include the fact that the BMO is a real anatomical entity, readily identified in OCT scans of the ONH and serves in the vast majority of instances as a true boundary of the canal through which all retinal ganglion cell axons pass.[8,9] The minimum distance from the BMO point across the neural rim (in this case to the nearest point along the inner limiting membrane segmentation) has the additional geometric advantage of being perpendicular to the trajectory of axon bundles as they traverse the ONH rim and enter the canal.

These potential advantages have proven to enhance clinical diagnosis by a meaningful margin over other common parameters including RNFL thickness.[10] The parameter BMO-MRW and the related parameter minimum rim area (MRA) also exhibit a stronger structure-function relationship with visual field sensitivity[11,12] and a stronger structure–structure relationship with peripapillary RNFL thickness (RNFLT)[11] compared to other ONH neuroretinal rim parameters. The ONH parameters MRW and MRA also are among the most sensitive for in vivo detection of the earliest manifestations of glaucomatous structural change as demonstrated in several longitudinal studies of nonhuman primates (NHP) with unilateral experimental glaucoma (EG).[13–16] Minimum rim width and MRA

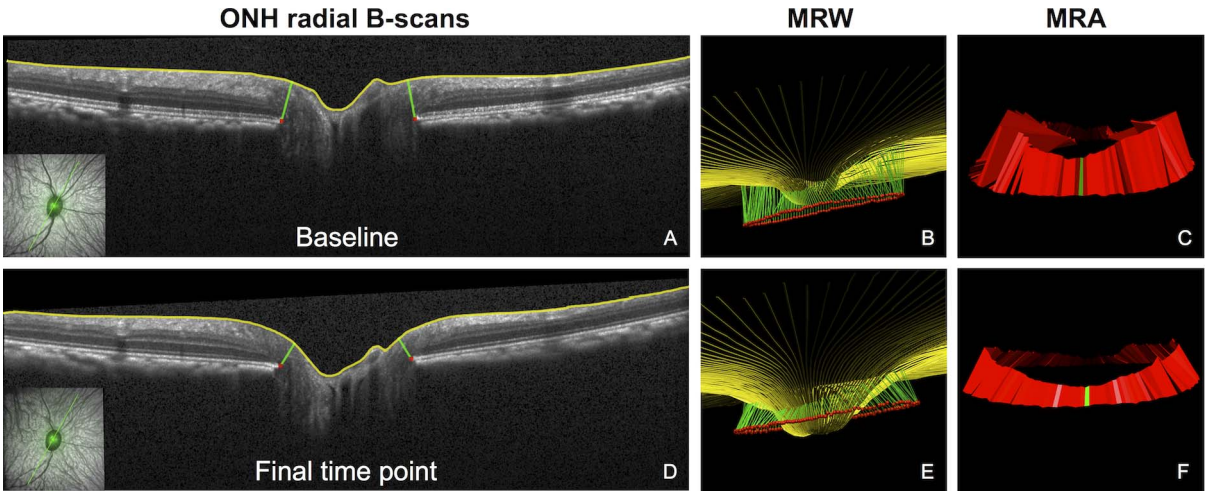

Figure 1. Segmentation of ONH radial scans. Individual example of an EG eye imaged at the first baseline (**A–C**) and at the final time point (**D–F**) just before euthanasia. *Insets* in the *lower left corner* of (**A**) and (**D**) show the location of the B-scan as indicated by the *bold green line* overlaid onto the infrared CSLO reflectance image. Structures delineated in each radial B-scan include the ILM, including the central meniscus of Kuhnt (*yellow*) and BMO points (*red*). The *green segments* connecting BMO points to the ILM represent the pair of MRW measurements made in each radial B-scan. Results for all 80 B-scans are shown in 3D for the baseline (**B**) and final time point (**E**). Note deformation of the ONH apparent in (**E**), including a deeper "cup" and thinner "rim." Global average MRW decreased from 330 μm at baseline to 200 μm at the final time point (−40%). Minimum rim area decreased from 1.11 mm^2 at baseline (**C**) to 0.69 mm^2 at the final time point ([**F**], −38%).

consistently have been shown to change before peripapillary RNFLT in NHP EG.[13–16]

This growing body of evidence suggests that the ONH parameters MRW and MRA might be better for assessment of structural changes in glaucoma than RNFLT. However, recent evidence also suggests that glaucomatous deformations of connective tissues, such as the lamina cribrosa and peripapillary sclera, exert a greater influence on ONH structure than on peripapillary RNFLT.[13,14,17,18] Although such connective tissue deformations are important to detect and monitor in glaucoma, they also might confound the degree to which ONH neuroretinal rim changes correlate with axon loss. In this regard, it is possible that RNFLT may provide a better surrogate measure of retinal ganglion cell axon loss than the ONH parameters MRW and MRA. Hence, there is interest in knowing the degree to which these relatively new in vivo measures of the ONH neuroretinal rim tissue might correlate with the number of retinal ganglion cell axons. Therefore, the purpose of this study was to compare spectral-domain OCT (SDOCT) measurements of ONH parameters MRW and MRA, as well as peripapillary RNFLT to complete orbital optic nerve axon counts in a NHP model of EG.

Methods

Subjects

The subjects of this study were 51 rhesus macaque monkeys (*Macaca mulatta*), 40 female and 11 male. At the start of the study, their age ranged from 1.2 to 22.6 years (median, 9.6 years) and their weight ranged from 3.3 to 13.9 kg (median, 5.9 kg). This study was done in strict accordance with the recommendations in the Guide for the Care and Use of Laboratory Animals of the National Institutes of Health and was approved and monitored by the Institutional Animal Care and Use Committee (IACUC) at Legacy Health. All experimental methods and animal care procedures also adhered to the Association for Research in Vision and Ophthalmology (ARVO) Statement for the Use of Animals in Ophthalmic and Vision Research.

Anesthesia

All experimental procedures began with induction of general anesthesia using ketamine (10–25 mg/kg IM) in combination with either xylazine (0.8-1.5 mg/kg intramuscularly [IM]) or midazolam (0.2 mg/kg IM), along with a single injection of atropine sulfate (0.05 mg/kg IM). Animals then were intubated with an endotracheal tube to breathe a mixture of 100% oxygen and air to maintain oxyhemoglobin saturation as close to 100% as possible. For all SDOCT imaging sessions, anesthesia after initial induction was maintained using isoflurane gas (1%–2%) mixed with 100% oxygen and delivered via endotracheal tube. A clear, rigid gas permeable contact lens filled with 0.5% carboxymethylcellulose solution was placed over the apex of each cornea. Intravenous fluids (lactated Ringer's solution, 10–20 mL/kg/h) were administered via the saphenous vein, vital signs were monitored throughout and recorded every 10 to 15 minutes, including heart rate, blood pressure, arterial oxyhemoglobin saturation, end tidal CO_2, and body temperature; body temperature was maintained at 37°C, heart rate above 75 beats per minute, and oxygen saturation above 95%.

IOP Measurements

Intraocular pressure was measured in both eyes at the start of every session using a Tonopen XL (Reichert Technologies, Inc., Depew, NY, USA). The value recorded for each eye was the average of three successive measurements.

SDOCT Imaging

All SDOCT scans were acquired using a Spectralis instrument (Heidelberg Engineering, GmbH, Heidelberg, Germany) 30 minutes after IOP was manometrically stabilized to 10 mm Hg. Spectral-domain OCT scans recorded at each session included an 80-radial B-scan pattern centered on the ONH (30° wide, 1536 A-scans/B-scan, Fig. 1) and a peripapillary circular B-scan with 12° diameter (1536 A-scans, Fig. 2). In all cases, 9 to 16 individual sweeps were averaged in real time to comprise the final stored B-scan at each session. The position of the scan was

Investigative Ophthalmology & Visual Science

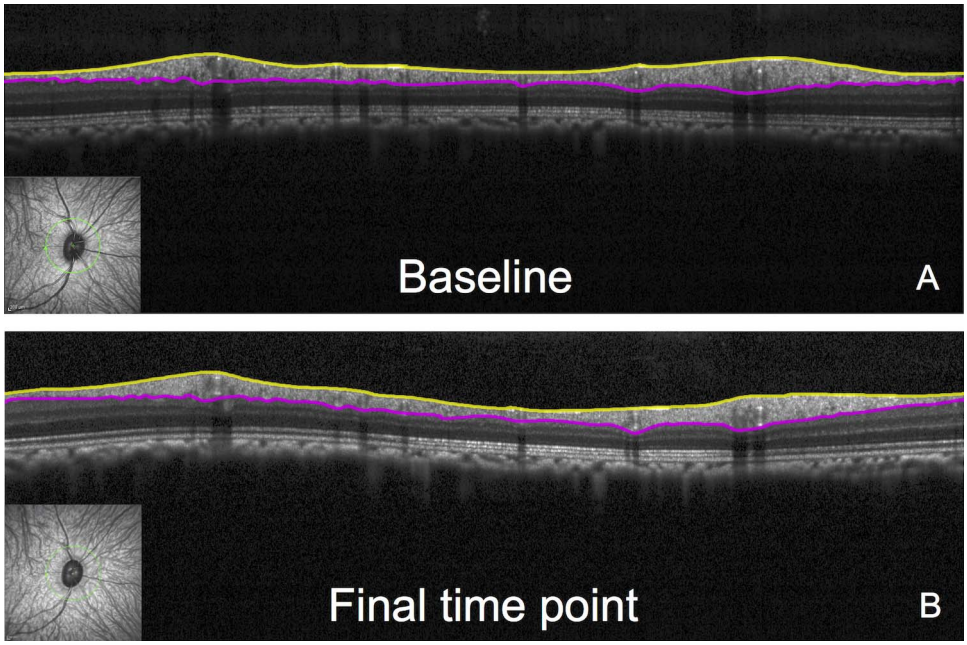

FIGURE 2. Segmentation of peripapillary circular B-scans. The individual example shown is the same EG eye and time points as in Figure 1 ([**A**], baseline; [**B**], final time point). Segmentations are shown for the ILM (*yellow*) and posterior RNFL boundary (*magenta*). Global average RNFLT decreased from 107.1 μm at baseline (**A**) to 82.9 μm at the final time point ([**B**], −23%).

centered on the ONH at the first imaging session and all follow-up scans were acquired at this same location using the instrument's automatic active eye tracking software. Image segmentation was performed manually using custom software (ATL 3D Suite). The ONH parameter MRW was derived from the radial ONH scans by determining the minimum distance from each Bruch's membrane opening (BMO) point to the inner limiting membrane (ILM) segmentation (Fig. 1), as described previously.[11,13,14] Minimum rim area was derived as the sum of the areas of 160 contiguous individual trapezoids whereby the base of each trapezoid is centered on the corresponding BMO point and the height of each trapezoid is defined as the distance between the BMO point and the ILM segmentation that minimizes the area of the trapezoid (Figs. 1C, 1F).

Peripapillary RNFLT was derived from the circular B-scan as the distance between the ILM and posterior RNFL segmentations (Fig. 2), as described previously.[17,19,20] In total, 605 ONH SDOCT volumes were analyzed in this study with a median scan quality score of 29.8 dB and interquartile range of 27.6 to 32.0 dB; the lowest scan quality score was 17.6 dB, which was the only value below 20 dB. The peripapillary circle scans had a median scan quality score of 31.3 dB and interquartile range of 27.9 to 34.3 dB; fewer than 1% had a score below 20 dB, the lowest of which was 13.9 dB.

Experimental Design and Protocol

Each animal had a minimum of three weekly baseline SDOCT imaging sessions (median number of prelaser baseline sessions, 5; average ± SD, 5.0 ± 1.6). Argon laser photocoagulation then was applied to the trabecular meshwork of one eye of each animal to induce chronic elevation of IOP.[21,22] Initially, 180° of the trabecular meshwork was treated in one session, then the remaining 180° was treated in a second session approximately 2 weeks later. If necessary, laser treatments were repeated in subsequent weeks (limited to a 90° sector) until an IOP elevation was first noted or if the initial postlaser IOP had returned to normal levels. The average number of laser treatments (± SD) was 5.6 ± 2.7.

After initiation of laser photocoagulation, repeat SDOCT imaging was performed approximately every 2 weeks. Imaging continued for each animal until its predefined target stage of damage severity had been reached. The specific target stage of EG for each animal was predetermined based on the primary study to which it was assigned. Thus, the EG stage at euthanasia differed across animals, providing a relatively wide range of damage for the cross-sectional analysis in this study. At endpoint, euthanasia occurred by pentobarbital overdose, optic nerve tissue was obtained for axon counts as described in the next section.

Optic Nerve Axon Counts

Complete (100%) axon counts were obtained from the retrobulbar optic nerve (Fig. 3).[20,23–26] Tissues were preserved by perfusion fixation with either 4% paraformaldehyde (N = 34) or 4% paraformaldehyde followed by 5% gluteraldehyde (N = 17). A 2 to 3 mm sample of each optic nerve, beginning 2 mm posterior to the globe, was cut with a vibratome (VT 100S; Leica Microsystems GmbH, Wetzlar, Germany) into 0.5-mm thick transverse sections. Each of these thick optic nerve sections was postfixed in 4% osmium tetroxide and embedded in epoxy resin. Optic nerve cross sections (1 μm thick) then were cut and stained with p-phenylenediamine and mounted on glass slides. The most complete and uniformly stained section from each optic nerve then was chosen for axon counting. Images covering 100% of the optic nerve cross section were automatically captured using an inverted light microscope (DM IRB; Leica Microsystems GmbH) with an oil immersion ×100 objective (PL Fluotar NA = 1.3; Leica Microsystems GmbH) and custom software for X-Y-Z stage control (Applied Scientific Instrumentation, Inc., Eugene, OR, USA) and image capture. Automated axon counting software[23] was used to count all of the axons with normal morphologic characteristics in each optic nerve cross-section. The total axon count for each optic nerve was represented by the sum of

Investigative Ophthalmology & Visual Science

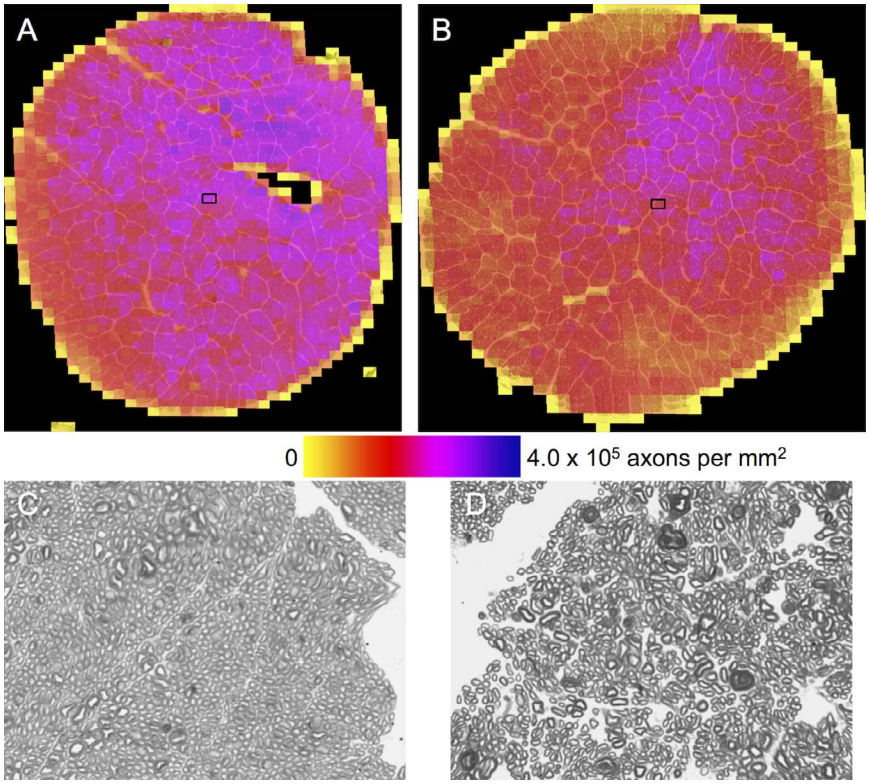

FIGURE 3. Optic nerve axon counts. All axons were counted from 100% of the cross-sectional area of each optic nerve. Shown here are the composited montages of all image tiles used to count axons for the control eye (**A**) and EG eye (**B**) of the same NHP shown in Figures 1 and 2. Axon density of each tile is color-coded, *insets* from (**A**) and (**B**), respectively, show a magnified view of a single tile in (**C**) and (**D**). Total axon count was 1,319,268 in the control eye and 1,001,512 in the EG eye (−24.1%).

all counted axons across all images tiling its entire cross-sectional area; axons falling within the 15%-overlap area between adjacent tiles were counted only once.

Analysis and Statistics

All statistical analysis was performed using a commercial software package (Prism 5; GraphPad Software, Inc., La Jolla, CA, USA). Pearson correlation coefficients were used to evaluate the strength of the relationship between each of the three SDOCT parameters and axon counts. Differences in the strength of correlation between each SDOCT parameter and the total axon count were compared using Steiger's test[27] whereby the null hypothesis is that no difference exists.

RESULTS

Study Duration and IOP

The total study duration ranged from 7 to 46 months (median, 13 months); the duration of postlaser follow-up ranged from 3 to 37 months (median, 8 months). In the group of 51 EG eyes, mean IOP over the span of postlaser follow-up ranged from 10.4 to 31.0 mm Hg (median, 19.6 mm Hg). Mean IOP over the same period in the fellow control eyes ranged from 8.4 to 23.3 mm Hg (median, 11.4 mm Hg). The peak IOP observed during the postlaser follow-up period ranged from 15.3 to 60.3 mm Hg in EG eyes (median, 43.0 mm Hg) and from 10.0 to 31.3 mm Hg in fellow control eyes (median, 15.3 mm Hg). The median time between the final imaging session and death was 5 days (range, 0–14 days).

Intereye Correlation of SDOCT Parameters at Baseline

Longitudinal in vivo measurements of SDOCT parameters enable estimates of damage severity to be made either by comparing the value at the final time point to the baseline average value within the same eye or by intereye comparison at the final time point. The latter may offer an excellent surrogate of the former when intereye correlation is otherwise strong before onset of damage ensues.[24] Since axon count data are only available at the final time point, the comparisons to in vivo measures of damage severity should be made on the same basis. Thus, it is important to evaluate the intereye correlation of each in vivo SDOCT parameter at baseline. Figure 4 shows that the intereye correlation between the two eyes of each animal at baseline was strong for all three SDOCT parameters. This correlation was significantly stronger for RNFLT (R = 0.973; 95% confidence interval [CI], 0.954–0.985) and MRW (R = 0.965; 95% CI, 0.939–0.980) than for MRA (R = 0.848, 95% CI, 0.748–0.911, $P < 0.0001$ each comparison, Steiger's test).

EG Eye Changes in SDOCT Parameters at the Final Time Point

The magnitude of SDOCT parameter change in EG eyes was similar when expressed relative to baseline or relative to control eye values at the final time point. In EG eyes, RNFLT was −21.7% relative to baseline on average (range, −63.8% to +9.1%), MRW was −38.2% (range, −87.7% to −4.4%), and MRA was −36.4% (range, −86.9% to −0.4%). The magnitude of longitudinal change was related to mean and peak postlaser IOP for all three parameters, but not to duration of postlaser

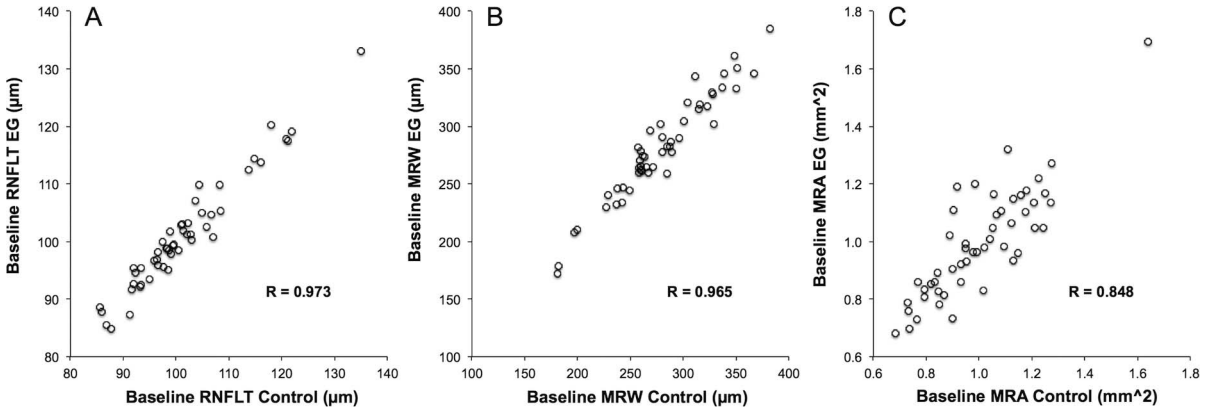

Figure 4. Intereye correlation of SDOCT parameters at baseline. The baseline average value for each eventual EG eye is plotted against the baseline average value of the fellow control eye for the SDOCT parameters RNFLT (**A**), MRW (**B**), and MRA (**C**). The Pearson correlation coefficient is listed in each Figure ($P < 0.0001$ in each case).

follow up, number of laser treatments or age (Supplementary Table S1). When loss in EG eyes is expressed relative to control eye values at the final time point, RNFLT was −21.8% on average (range, −64.2% to +6.0%), MRW was −37.5% (range, −87.1% to −4.5%), and MRA was −36.4% (range, −85.9% to +3.9%), all very close to the estimates of loss based on longitudinal change from baseline. This supports the comparison to axon loss based on intereye differences. The average optic nerve axon loss expressed in the same manner was −36.3% (range, −82.1% to +5.4%) relative to fellow control eye values.

The baseline data were further used to support an event analysis for comparing the relative diagnostic capability of each parameter. First, a bootstrap analysis of all possible within-eye pairs of baseline observations was applied to determine the 95% limits-of-agreement for each parameter. This range was ±7% of baseline average values for RNFLT (identical to previous analyses of overlapping datasets),[17,19,28] ±12% of baseline average for MRW, and ±12% of baseline average for MRA, indicating that the ONH parameters are more variable than RNFLT in the absence of disease. These data then were used as a basis to determine the proportion of EG eyes demonstrating significant longitudinal change (i.e., beyond the 95% limits-of-agreement) at the final time point (akin to diagnostic "sensitivity") and the proportion of fellow control eyes demonstrating significant longitudinal change at the final time point (akin to diagnostic "specificity"). The results of this analysis reveal that at the final time point, 38 EG eyes (75%) had a significant RNFLT decline from baseline, 46 (90%) had significant MRW decline, and 45 (88%) had significant MRA decline. The proportion of EG eyes with significant change from baseline was higher for MRW ($P = 0.02$) and MRA ($P = 0.04$) compared to RNFLT. None of the control eyes had any significant change from baseline at the final time point, indicating an equivalent specificity of 100% for all three parameters. These latter results are consistent with the fact that at the final imaging session, there was no difference from baseline in the control eye group for values of RNFLT ($P = 0.96$), MRW ($P = 0.50$), or MRA ($P = 0.78$).

Correlation Between SDOCT Parameters and Optic Nerve Axon Count

The correlation with axon counts was strongest for RNFLT ($R = 0.81$; 95% CI, 0.73–0.87), compared to either MRW ($R = 0.72$; 95% CI, 0.61–0.80) or MRA ($R = 0.70$; 95% CI, 0.59–0.79; $P < 0.01$ for each comparison; Fig. 5). This also was true if only EG eyes were considered ($P < 0.05$ for each comparison). There was no significant difference, however, between the correlation of MRW to axon count and the correlation of MRA to axon count ($P = 0.43$). Comparing across the three panels of Figure 5 also reveals that there is less overlap between EG and control

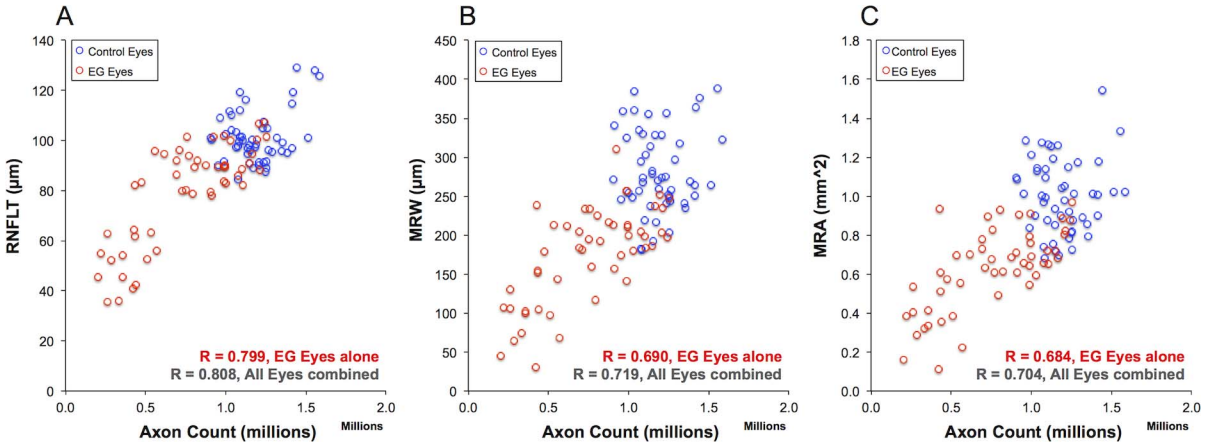

Figure 5. Correlation between SDOCT parameters at final time point and axon count. Spectral-domain OCT parameter values are plotted versus axon count for each individual eye in the study; RNFLT (**A**), MRW (**B**), and MRA (**C**). Pearson correlation coefficients are listed in each Figure ($P < 0.0001$ in all cases).

Investigative Ophthalmology & Visual Science

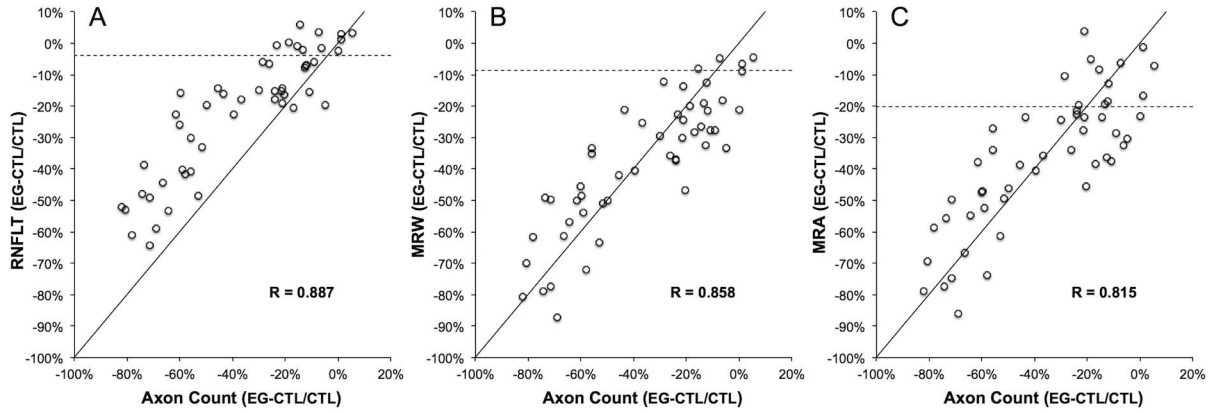

Figure 6. Correlation between severity of loss measured by SDOCT parameters at final time point and axon loss. Spectral-domain OCT parameter values in each EG eye at the final time point are expressed relative to the value in the fellow control eye at the final time point and plotted versus relative axon count; RNFLT (**A**), MRW (**B**), and MRA (**C**). Pearson correlation coefficients are listed in each Figure ($P < 0.0001$ in each case). The *dashed horizontal line* in each Figure represents the lower end of the range encompassing 95% of the intereye differences at baseline (i.e., the lower boundary of the normal range of intereye differences). The *diagonal line* in each Figure represents the 1:1 locus.

eyes for MRW and MRA at low levels of axon loss compared to RNFLT. For example, only 43 EG eyes (84%) had a final value of RNFLT below the median value for control eyes, whereas 50 (98%, $P = 0.006$) and 51 (100%, $P = 0.001$) EG eyes, respectively, had final MRW and MRA values below the control eye median. The EG eyes (red points) tend to shift downward relative to control eyes (blue points) for MRW and MRA, whereas the EG eyes tend to shift leftward relative to control eyes for RNFLT, indicating that axon loss occurs before manifestation of loss by RNFLT. This lag for RNFLT is shown more clearly by comparison of relative loss based on intereye analysis in the next section.

The correlation between relative RNFLT loss and relative axon loss ($R = 0.89$) was not significantly stronger than that for MRW ($R = 0.86$, $P = 0.17$, Steiger's test), but both were significantly stronger than MRA ($R = 0.81$; $P = 0.02$ each comparison, Steiger's test; Fig. 6). The data in Figure 6 also exhibit the phenomenon whereby relative loss of RNFLT is shifted leftward (of the 1:1 line) indicating a "delay" relative to axon loss, whereas the data for MRW and MRA are scattered more symmetrically about the 1:1 line.

Discussion

The purpose of this study was to compare the relationship between complete orbital optic nerve axon counts and SDOCT measurements of two relatively new ONH parameters, MRW and MRA, as well as to the more widely used parameter peripapillary RNFLT. We found that although the ONH parameters MRW and MRA were more sensitive than peripapillary RNFLT in terms of detecting glaucomatous structural changes, RNFLT was correlated more closely with total orbital optic nerve axon counts. We confirmed earlier findings that demonstrate a "delay" between early-stage axon loss and the first manifestation of RNFLT loss (Figs. 5, 6),[24,25] whereas the ONH parameters MRW and MRA begin to separate from control values at the earliest stage of axon loss. This inference, based on cross-sectional analyses of longitudinal data in this study, is supported by results of previous studies, some of which applied longitudinal analyses.[13–16] These results also are consistent with the recent report that clinical diagnosis of glaucoma was enhanced by use of the parameter MRW compared to RNFLT.[10] It is likely that the diagnostic advantages offered by the ONH parameters MRW and MRA, compared to RNFLT, reflect the fact that ONH connective tissue deformation and remodeling have a greater influence on the ONH parameters MRW and MRA than on RNFLT. A similar explanation has been proposed to account for the greater sensitivity of ONH surface topography over RNFLT.[17]

Nevertheless, MRW and MRA proved to be nearly twice as variable in the healthy state (i.e., during baseline) as RNFLT in this laboratory setting, which likely persisted through a wide range of damage and contributed to the weaker correlations of MRW and MRA to axon counts (Fig. 5). The larger test–retest variability of MRW and MRA also may explain their larger intereye variability, MRA especially, compared to RNFLT (Figs. 4, 6). These results are not unique to EG in a laboratory setting as evidenced by the recent findings from Gardiner et al.[29] based on clinical study data, who reported that: "RNFLT measured by SDOCT had a better longitudinal signal-to-noise ratio than MRW or MRA. Although MRW and MRA may be more sensitive for early detection of glaucomatous damage, these data suggest that RNFLT may be preferable for monitoring change."[29] In fact, it is likely that the ONH parameters MRW and MRA are hindered (relative to RNFLT) even more in the clinical setting than in our laboratory studies, since we control IOP manometrically at the time of SDOCT imaging, whereas this is not done clinically. This is relevant because ambient IOP has a greater influence on ONH parameters, such as MRW and MRA, than it does on RNFLT measured 6° into the peripapillary retina.[30,31]

An important caveat to consider is that in some ONH sectors of some eyes, the MRW vector crosses elements of middle and outer retinal layers that "protrude" into the rim as defined by the minimum distance between the BMO and ILM. Figure 7 provides an example from a healthy eye of one NHP (this also occurs in human eyes). In this example, more than half of the width of the nasal rim defined by MRW may consist of inner and outer nuclear layers, outer plexiform layer, and perhaps also some inner plexiform layer tissue. This anatomical variant may contribute to the weaker correlations observed between ONH parameters and axon counts compared to RNFLT. It also is possible that differences exist among healthy eyes in the proportion of other nonaxonal components occupying these tissues, such as capillaries, larger blood vessels, and glia. Some or all of these nonaxonal components also may vary in the degree to which they change during the course of glaucomatous damage to individual eyes.

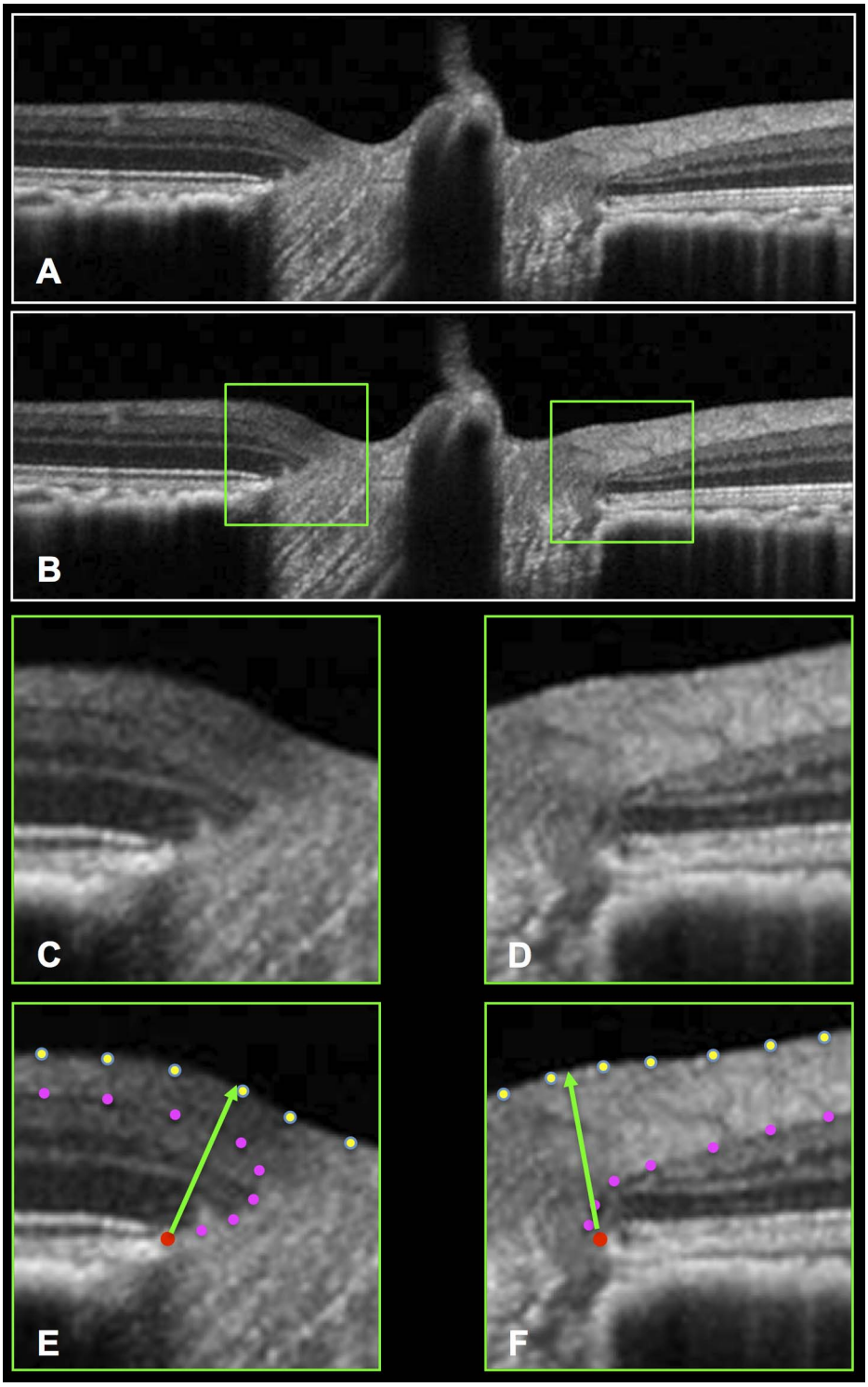

FIGURE 7. While the ONH neuroretinal rim tissue and peripapillary RNFL contain retinal ganglion cell axons, glia, and blood vessels, the neuroretinal rim defined by the minimum distance between BMO and ILM also can contain outer and middle retinal layers. (**A**) Horizontal B-scan through the ONH of a representative healthy monkey eye (nasal *left*, temporal *right*). (**B**) Same B-scan showing locations outlined by *green boxes* for magnified views shown without segmentations in (**C**) and (**D**) and with segmentations in (**E**) and (**F**): ILM (*yellow dots*), posterior boundary of RNFL and border between retina and axon bundles of the prelaminar ONH (*magenta dots*), BMO points (*red dots*), and MRW vectors (*green arrows*). In this example, middle and outer retinal layers are present in the nasal rim (more than half the total width) and temporal rim (to a lesser extent).

The limitations of this study revolve around the issue of generalizability. This study was done in an EG model that is based solely on chronic IOP elevation; no other variables, such as genetic risk factors or cardiovascular health, are scientifically controlled. It is possible that the greater complexity of human clinical glaucoma would alter the relationships we observed. Moreover, the monkey ONH may be more malleable than the human ONH, which might

further complicate generalization of our observations to the clinical realm.

In summary, RNFLT was correlated more strongly with complete orbital axon counts than MRW or MRA, though the ONH parameters were more sensitive for detection of glaucomatous structural damage. These findings likely derive from the fact that glaucomatous deformation of ONH connective tissue structures (separate from axon loss alone) is reflected more by MRW and MRA than by RNFLT and also that measurements of these ONH parameters are more variable than RNFLT.

Acknowledgments

The authors thank Galen Williams and Luke Reyes for their expert technical assistance during data collection and tissue processing.

Supported by National Institutes of Health (NIH; Bethesda, MD, USA) NIH R01-EY019327 (BF), R01-EY011610, and R01-EY021281 (CFB), R01-EY019939 (LW); Legacy Good Samaritan Foundation; Heidelberg Engineering, GmbH, Heidelberg, Germany (equipment and unrestricted research support).

Disclosure: **B. Fortune**, None; **C. Hardin**, None; **J. Reynaud**, None; **G. Cull**, None; **H. Yang**, None; **L. Wang**, None; **C.F. Burgoyne**, Heidelberg Engineering GmbH (F, C, R)

References

1. Sharma P, Sample PA, Zangwill LM, Schuman JS. Diagnostic tools for glaucoma detection and management. *Surv Ophthalmol*. 2008;53(suppl 1):S17–S32.
2. Leung CK. Diagnosing glaucoma progression with optical coherence tomography. *Curr Opin Ophthalmol*. 2014;25: 104–111.
3. Bussel II, Wollstein G, Schuman JS. OCT for glaucoma diagnosis, screening and detection of glaucoma progression. *Br J Ophthalmol*. 2014;98(suppl 2):ii15–19.
4. Fortune B. In vivo imaging methods to assess glaucomatous optic neuropathy. *Exp Eye Res*. 2015;141:139–153.
5. Chauhan BC, Burgoyne CF. From clinical examination of the optic disc to clinical assessment of the optic nerve head: a paradigm change. *Am J Ophthalmol*. 2013;156:218–227.
6. Povazay B, Hofer B, Hermann B, et al. Minimum distance mapping using three-dimensional optical coherence tomography for glaucoma diagnosis. *J Biomed Opt*. 2007;12:041204.
7. Chen TC. Spectral domain optical coherence tomography in glaucoma: qualitative and quantitative analysis of the optic nerve head and retinal nerve fiber layer (an AOS thesis). *Trans Am Ophthalmol Soc*. 2009;107:254–281.
8. Reis AS, O'Leary N, Yang H, et al. Influence of clinically invisible, but optical coherence tomography detected, optic disc margin anatomy on neuroretinal rim evaluation. *Invest Ophthalmol Vis Sci*. 2012;53:1852–1860.
9. Reis AS, Sharpe GP, Yang H, Nicolela MT, Burgoyne CF, Chauhan BC. Optic disc margin anatomy in patients with glaucoma and normal controls with spectral domain optical coherence tomography. *Ophthalmology*. 2012;119:738–747.
10. Chauhan BC, O'Leary N, Almobarak FA, et al. Enhanced detection of open-angle glaucoma with an anatomically accurate optical coherence tomography-derived neuroretinal rim parameter. *Ophthalmology*. 2013;120:535–543.
11. Gardiner SK, Ren R, Yang H, Fortune B, Burgoyne CF, Demirel S. A method to estimate the amount of neuroretinal rim tissue in glaucoma: comparison with current methods for measuring rim area. *Am J Ophthalmol*. 2014;157:540–549.
12. Danthurebandara VM, Sharpe GP, Hutchison DM, et al. Enhanced structure-function relationship in glaucoma with an anatomically and geometrically accurate neuroretinal rim measurement. *Invest Ophthalmol Vis Sci*. 2015;56:98–105.
13. Strouthidis NG, Fortune B, Yang H, Sigal IA, Burgoyne CF. Longitudinal change detected by spectral domain optical coherence tomography in the optic nerve head and peripapillary retina in experimental glaucoma. *Invest Ophthalmol Vis Sci*. 2011;52:1206–1219.
14. He L, Yang H, Gardiner SK, et al. Longitudinal detection of optic nerve head changes by spectral domain optical coherence tomography in early experimental glaucoma. *Invest Ophthalmol Vis Sci*. 2014;55:574–586.
15. Patel NB, Sullivan-Mee M, Harwerth RS. The relationship between retinal nerve fiber layer thickness and optic nerve head neuroretinal rim tissue in glaucoma. *Invest Ophthalmol Vis Sci*. 2014;55:6802–6816.
16. Ivers KM, Sredar N, Patel NB, et al. In vivo changes in lamina cribrosa microarchitecture and optic nerve head structure in early experimental glaucoma. *PLoS One*. 2015; 10:e0134223.
17. Fortune B, Reynaud J, Wang L, Burgoyne CF. Does optic nerve head surface topography change before loss of retinal nerve fiber layer thickness: a test of the site of injury hypothesis in experimental glaucoma. *PLoS One*. 2013;8:e77831.
18. Xu G, Weinreb RN, Leung CK. Optic nerve head deformation in glaucoma: the temporal relationship between optic nerve head surface depression and retinal nerve fiber layer thinning. *Ophthalmology*. 2014;121:2362–2370.
19. Fortune B, Burgoyne CF, Cull G, Reynaud J, Wang L. Onset and progression of peripapillary retinal nerve fiber layer (RNFL) retardance changes occur earlier than RNFL thickness changes in experimental glaucoma. *Invest Ophthalmol Vis Sci*. 2013; 54:5653–5661.
20. Fortune B, Cull G, Reynaud J, Wang L, Burgoyne CF. Relating retinal ganglion cell function and retinal nerve fiber layer (RNFL) retardance to Progressive Loss of RNFL thickness and optic nerve axons in experimental glaucoma. *Invest Ophthalmol Vis Sci*. 2015;56:3936–3944.
21. Gaasterland D, Kupfer C. Experimental glaucoma in the rhesus monkey. *Invest Ophthalmol*. 1974;13:455–457.
22. Quigley HA, Hohman RM. Laser energy levels for trabecular meshwork damage in the primate eye. *Invest Ophthalmol Vis Sci*. 1983;24:1305–1307.
23. Reynaud J, Cull G, Wang L, et al. Automated quantification of optic nerve axons in primate glaucomatous and normal eyes–method and comparison to semi-automated manual quantification. *Invest Ophthalmol Vis Sci*. 2012;53:2951–2959.
24. Cull GA, Reynaud J, Wang L, Cioffi GA, Burgoyne CF, Fortune B. Relationship between orbital optic nerve axon counts and retinal nerve fiber layer thickness measured by spectral domain optical coherence tomography. *Invest Ophthalmol Vis Sci*. 2012;53:7766–7773.
25. Cull GA, Reynaud J, Wang L, Cioffi GA, Burgoyne CF, Fortune B. Erratum in: "Relationship between orbital optic nerve axon counts and retinal nerve fiber layer thickness measured by spectral domain optical coherence tomography." *Invest Ophthalmol Vis Sci*. 2014;55:2619–2620.
26. Fortune B, Reynaud J, Cull G, Burgoyne CF, Wang L. The effect of age on optic nerve axon counts, SDOCT scan quality, and peripapillary retinal nerve fiber layer thickness measurements in rhesus monkeys. *Transl Vis Sci Technol*. 2014;3:2.
27. Steiger JH. Tests for comparing elements of a correlation matrix. *Psychol Bull*. 1980;87:245–251.
28. Fortune B, Burgoyne CF, Cull GA, Reynaud J, Wang L. Structural and functional abnormalities of retinal ganglion cells measured in vivo at the onset of optic nerve head surface change in experimental glaucoma. *Invest Ophthalmol Vis Sci*. 2012;53:3939–3950.

29. Gardiner SK, Boey PY, Yang H, Fortune B, Burgoyne CF, Demirel S. Structural measurements for monitoring change in glaucoma: comparing retinal nerve fiber layer thickness with minimum rim width and area. *Invest Ophthalmol Vis Sci*. 2015;56:6886–6891.
30. Fortune B, Yang H, Strouthidis NG, et al. The effect of acute intraocular pressure elevation on peripapillary retinal thickness, retinal nerve fiber layer thickness, and retardance. *Invest Ophthalmol Vis Sci*. 2009;50:4719–4726.
31. Strouthidis NG, Fortune B, Yang H, Sigal IA, Burgoyne CF. Effect of acute intraocular pressure elevation on the monkey optic nerve head as detected by spectral domain optical coherence tomography. *Invest Ophthalmol Vis Sci*. 2011;52:9431–9437.

Investigative Ophthalmology & Visual Science